

Nonlinear particle motion and bursty periodic energy deposition in inductively coupled plasmas

Haomin Sun¹, Jian Chen^{2,*}, Alexander Khrabrov³, Igor D.
Kaganovich³, Wei Yang⁴, Dmytro Sydorenko⁵, Stephan Brunner¹

¹*Ecole Polytechnique Fédérale de Lausanne (EPFL),*

Swiss Plasma Center (SPC), CH-1015 Lausanne, Switzerland

²*Sino-French Institute of Nuclear Engineering and Technology,
Sun Yat-sen University, Zhuhai 519082, People's Republic of China*

³*Princeton Plasma Physics Laboratory,*

Princeton University, Princeton, New Jersey 08543, USA

⁴*College of Physics, Donghua University,*

Shanghai 201620, People's Republic of China

⁵*University of Alberta, Edmonton, Alberta T6G 2E1, Canada*

(Dated: March 6, 2025)

Abstract

Two-dimensional electromagnetic particle-in-cell simulations are employed to study particle motion and power deposition in inductively coupled plasmas. We show that under condition of low-frequency (\sim MHz) and low-pressure, the electron motion is highly nonlinear in the skin region near the coil: electrons are strongly magnetized, and the energy deposition is small throughout most of the RF cycle. However, during the phase when the RF magnetic field vanishes, electrons briefly demagnetize, causing a jet-like current penetrating into the plasma. During these short time intervals the power deposition becomes high, resulting in periodic bursts in the energy deposition. We developed a new kinetic theory, which not only provides analytical expressions for the plasma current and energy deposition, but also predicts a new nonlinear relation between electron current and the RF inductive electric field. A criterion for transition between the low frequency, periodic bursty nonlinear regime and the high frequency, anomalous non-local skin effect regime is proposed and verified using a series of fully kinetic 2D particle-in-cell simulations.

Introduction—Energy deposition into electrons by time-varying electromagnetic field is the primary method of sustaining gas discharge in material processing reactors [1, 2], such as Capacitively Coupled Plasma (CCP) [3–8] and Inductively Coupled Plasma (ICP) discharges [9–13]. Driven by industry demands to achieve atomic-scale precision, plasma processing systems tend to operate at low gas pressure (several mTorr) [3, 6, 14–18], making it crucial to understand the electron dynamics in the plasma [19, 20]. For low pressure, high frequency ($f = 13.56$ MHz or higher) ICP discharges, it was determined that the skin effect is anomalous [21–30], meaning that the skin depth, δ , is determined by non-local kinetics as $\delta \sim (v_{th}c^2/\omega\omega_{pe}^2)^{1/3}$ instead of $\delta \sim c/\omega_{pe}$ for the normal skin effect, where v_{th} is the electron thermal velocity, c is the speed of light, ω is the driving frequency, and ω_{pe} is the electron plasma frequency. The electron heating in this anomalous regime is mainly due to wave-particle resonance of low energy electrons, which can be treated similarly to the Landau damping [10, 19, 30–35]. The anomalous regime had also been called the non-local regime because over one RF period the electrons travel a significant distance $d \sim v_{th}/\sqrt{\omega^2 + \nu^2} > \delta$ [30], where ν is the collision frequency. As a result, the plasma current is a non-local function of the RF electric field, and the RF field penetrates deeper into the plasma and deposits its

energy over a wider region in the plasma. Multiple modeling studies have been performed for the ICP discharges utilizing the non-local kinetic approach [19, 31, 36–41], predicting the spatial distribution of the plasma current as well as the resulting energy deposition into the plasma.

Although ICP discharge systems operate mostly at high frequency [42, 43], it has been recently shown that operating an ICP discharge at lower frequency (~ 1 MHz) has certain advantages [44–47]. At low frequency, the capacitive coupling with the plasma can be reduced [48], the external circuit losses decrease [48, 49], and a higher power transfer efficiency can be achieved [45], thereby improving the overall performance of plasma processing systems. A more complicated ICP operation using pulsed waveforms [50–56] also requires a fundamental understanding of ICP operation at low frequency. Low-frequency ICP discharges are also used as sources for negative ion beams for fusion applications due to improved plasma uniformity [57–60].

At the same time, due to the lack of a self-consistent kinetic 2D modeling, the physics of low-frequency ICP discharges is not sufficiently understood. Although it was previously shown that at low frequencies the particle dynamics could become highly nonlinear due to RF magnetic field [46, 61, 62], these studies are based on simplified single particle analysis. Despite the work classifying ICP discharges according to estimated skin depth [63], the electron gyro-radius was assumed to be much larger than the skin depth and it is still necessary to more carefully analyze the particle dynamics by self-consistent numerical simulations. Moreover, many existing kinetic simulations [37, 64–68] are mostly limited to 1D or high frequency ICP discharges. More importantly, to the best of our knowledge, a theory that can explain the particle dynamics and electron current in low frequency ICP as observed in our simulations has been lacking. Therefore, a comprehensive numerical and analytical study is necessary to understand the relevant physics of the particle dynamics and energy deposition in low-frequency ICP discharges.

We present the first comprehensive electromagnetic 2D PIC simulations of a low frequency ICP discharge. We show that a strongly nonlinear skin effect regime with periodic bursty energy deposition is attained at relatively low RF frequency. In such a regime, electrons are magnetized and power deposition is low during most of the RF period. Demagnetization occurs when the RF magnetic field passes through zero, and electrons quickly leave area near antennas and form a current jet propagating into the plasma, causing periodic bursts

in the energy deposition. A new kinetic theory is developed and predicts well the plasma current in this bursty regime.

Method—We develop and employ the electromagnetic Darwin version of the two-dimensional particle code EDIPIC-2D [16, 17, 69–73] to simulate an inductively coupled discharge, with antenna coils positioned at the top of the chamber [74]. Figures 1 (a2) and (b2) show the simulation domain. The chamber dimensions are $D_x \times D_y = 80 \text{ mm} \times 80 \text{ mm}$, with a dielectric slab located at $70 \text{ mm} < y < 80 \text{ mm}$ with antennas positioned inside the dielectric as indicated by black rectangles and plasma occupying the rest of the chamber volume. The simulations are performed in Cartesian geometry for ease of analysis. Because the code implements a direct-implicit time advance [6, 64, 75, 76], we set the cell size to $\Delta x = 0.33 \text{ mm}$, resulting in grid dimensions of $n_x \times n_y = 240 \times 240$. The antenna currents have a 180° phase difference, with the frequency $f = \omega/2\pi$ in the range of 1 to 10 MHz and the amplitude $I_{coil} = 60$ to 280 A. The amplitude of the coil current is relatively high because the plasma can be sustained only by such a current. This high current has been used in many ICP systems [23, 24, 77]. The domain boundaries are conductive, with secondary emission neglected. Initially, the system contains Argon gas at the pressure $p = 5 \text{ mTorr}$ and plasma with a uniform density $N_e = N_i = 10^{17} \text{ m}^{-3}$, electron temperature $T_e = 2.0 \text{ eV}$, and ion temperature $T_i = 0.03 \text{ eV}$. 1000 macro-particles per cell are set initially for all species. Each simulation runs for at least 3000 RF periods to make sure that a steady-state is reached.

Results—We first focus on two cases, with I_{coil} at 130A and frequencies of $f = 1 \text{ MHz}$ and $f = 10 \text{ MHz}$. Figure 1 shows the time histories and spatial profiles of the plasma for these two cases. The time evolution of the ion density and electron temperature shown in Figs. 1 (a1) and (b1) indicates that the simulations have reached a steady state. Subplots (a2) and (b2) show the magnetic field lines with superimposed colormaps of the field strength. We see that the magnetic field strength is almost the same between the low- and the high-frequency cases, because it depends mainly on the coil current ($B \propto I_{coil}$). Comparing the ion density profiles in Figs. 1 (a3) and (b3), we see a nearly two orders of magnitude difference. This is due to a comparable difference in energy deposition between (a4) and (b4), because $E_z \cdot J_{ze} \propto \omega^2 I_{coil}$.

A close examination of the current profiles of the two cases shown in Figs. 2 (a1) and (b1) reveals two notable distinctions. First, a well defined jet-like structure of the electron current

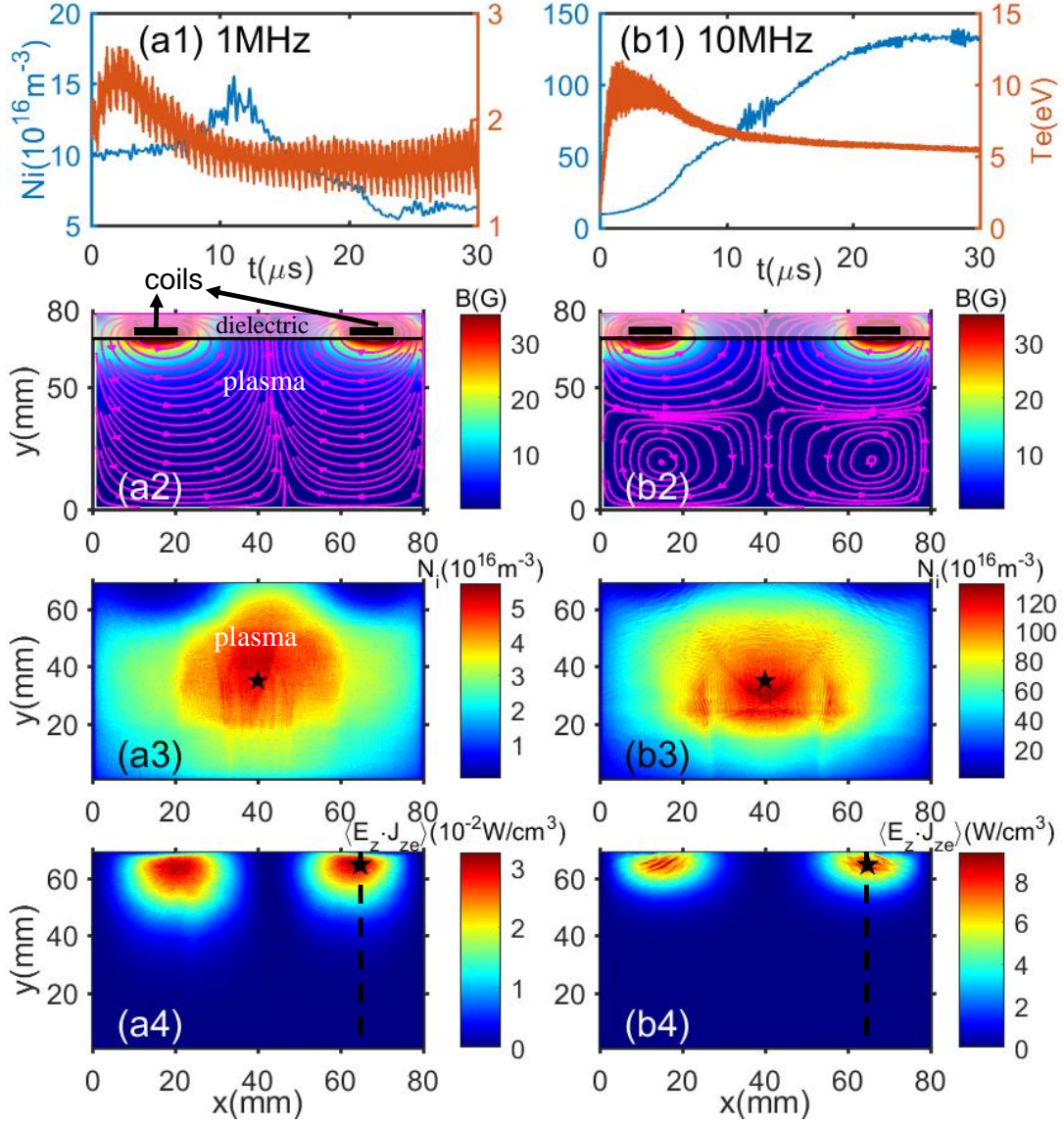


FIG. 1. Time evolution of physical quantities and steady-state profiles. Panel (a) is for the low frequency case $f = 1\text{MHz}$ and panel (b) is for the $f = 10\text{MHz}$ case. Subplots (a1) and (b1) show time evolution of the ion density and electron temperature. The probes are placed at the center, shown by black stars in (a3) and (b3). Subplots (a2) and (b2) show 2D maps of the magnetic field strength with superimposed magenta curves denoting the field lines. Black rectangles are the cross-sections of the coil wires, and the black horizontal line is the boundary between the plasma and the dielectric. The profiles in (a2) and (b2) are plotted at the phase when the RF magnetic field is at the maximum. The profiles in (a3)-(b4) are the time averaged ion density and energy deposition.

is observed in the time history for the low frequency case but not for the high frequency. The jet-like structure propagates into the plasma at around $t = 29.5\mu s$, with a speed close to the electron thermal velocity v_{th} , whereas no such a structure is observed in the $f = 10$ MHz case.

The second distinction is in the sample particle trajectories shown in Figs. 2 (a2) and (b2) for low and high frequency cases, respectively. For low frequency case, electrons are magnetized with a gyro-radius ($\sim 1.5\text{mm}$) smaller than the skin depth (~ 10 mm) and follow the RF magnetic field line. The electrons are however not magnetized in high frequency case. To trace the electrons, we seed 400 test particles with random initial velocity direction and velocity amplitude at $x = 68.0$ mm and $y = 65.7$ mm (marked by the black stars in Fig. 1 (a4) and (b4)) and $t = 29.2 \mu s$. The reason why we choose this location is because for our 1 MHz case, most new electrons are produced by ionization near the coil region (see Fig. 4 in our accompanying paper [78]). Among all the particles that were tracked in the simulation of the $f = 1$ MHz case, around 80% follow a trajectory similar to the one shown in Fig. 2 (a2). A movie showing time evolution of physical quantities at the electron's location is available in the supplemental material [79]. This is in significant contrast to the findings of previous work [63], where the Larmor radius was assumed to be much larger than the skin depth. It is evident from the Fig. 2 (a2) that the electron is magnetized and follow the magnetic field line. The oscillations of v_y and v_x shown in (a3) indicates that the electron undergoes a cyclotron motion in y direction and bounces parallel to the magnetic field in x direction. It is important to note that the electrons' y locations remain almost unchanged because of the plasma generated ambipolar electric field, E_y , which is caused by the charge separation driven by the magnetic part of the Lorentz force $\vec{v}_z \times \vec{B}$ acting on electrons; this electric field E_y counter balances the magnetic part of the Lorentz force, so that the total averaged force on electrons vanishes (see also Fig. 5 (d) and Ref. [78]). Figure 2 (a3) further shows that the particle motion in z direction is due to particle drifts, where $E_y \times B_x$ drift is the dominant one. As the RF magnetic field is out of phase with the RF electric field and it decreases with the increase of RF electric field, electrons eventually demagnetize during the phase when the magnetic field becomes small, electrons stop following the magnetic field lines and move into the plasma interior at around $t = 29.5 \mu s$, forming a jet-like structure shown in subplot (a1). During this process, the electron's canonical momentum $m_e v_z + eA$ is conserved (denoted by the light blue line in Fig. 2 (a3)), where A is the vector potential. A sample test particle in

the $f = 10$ MHz case, however, travels over the entire simulation domain during the 10 RF periods shown in the figure, interacting with the coil field transiently, as already described by many previous studies, see e.g., Refs. [61, 62].

To better understand the representative electron trajectory shown in Fig. 2 (a3), we consider a simplified 1D model of electron trajectory along the vertical dashed line in Fig. 1 (a4)). Note that the electron motion parallel to magnetic field is not considered. Here the vector potential can be approximated as $A_z(y, t) = A_{max} \exp(-y/\delta) \cos(\omega t)$ (where δ is the skin depth), with $B_x(y, t) = \partial A_z / \partial y$ and $E_z(y, t) = -\partial A_z / \partial t$ are the RF magnetic field in the x direction, and the RF inductive electric field in the z direction, respectively. The electron motion equation reads

$$m_e \frac{dv_y}{dt} = qv_z B_x - q \frac{\partial \Phi}{\partial y}, \quad m_e \frac{dv_z}{dt} = qE_z - qv_y B_x, \quad (1)$$

where Φ is the in-plane electrostatic potential describing ambipolar electric field $E_y(y, t)$. This indicates that for our cases, electrons do not follow pure cyclotron motion. Their trajectories are also affected by the electrostatic potential in the $x - y$ plane. Using the conservation of canonical momentum $m_e v_z + eA_z = const$, we can combine these two equations and obtain [61, 62]

$$\frac{d^2 y}{dt^2} = \frac{q}{m_e} \frac{\partial A_z}{\partial y} (v_{z0} - \frac{q}{m_e} (A_z - A_{z0})) - \frac{q}{m_e} \frac{\partial \Phi}{\partial y} \equiv -\frac{q}{m_e} \frac{\partial U}{\partial y}, \quad (2)$$

where A_{z0} is the vector potential at the initial time and position of the electron being considered and we define effective potential

$$U = q \frac{A_z^2}{2} - (qA_{z0} + m_e v_{z0}) A_z + \Phi. \quad (3)$$

Figure 3 shows the time evolution of the effective potential and the phase space trajectory of an example test particle obtained by numerically solving Eq. (2). The electrostatic potential and vector potential profile data is taken directly from the PIC simulation results. It is evident that the basic features of the trajectory shown in Fig. 2 (a3) are reproduced for the 1D trajectory shown in Fig. 3 (b). Therefore, electrons being produced near the coil are trapped in the effective potential well, while being accelerated in z direction. The bounce frequency Ω in the effective potential well is nearly the same as the local electron cyclotron frequency $\Omega_B = qB/m_e$ (see discussion in Ref. [78]). It is important to note that the turning points of the bounce motion stay almost unchanged with time, so average electron flux in

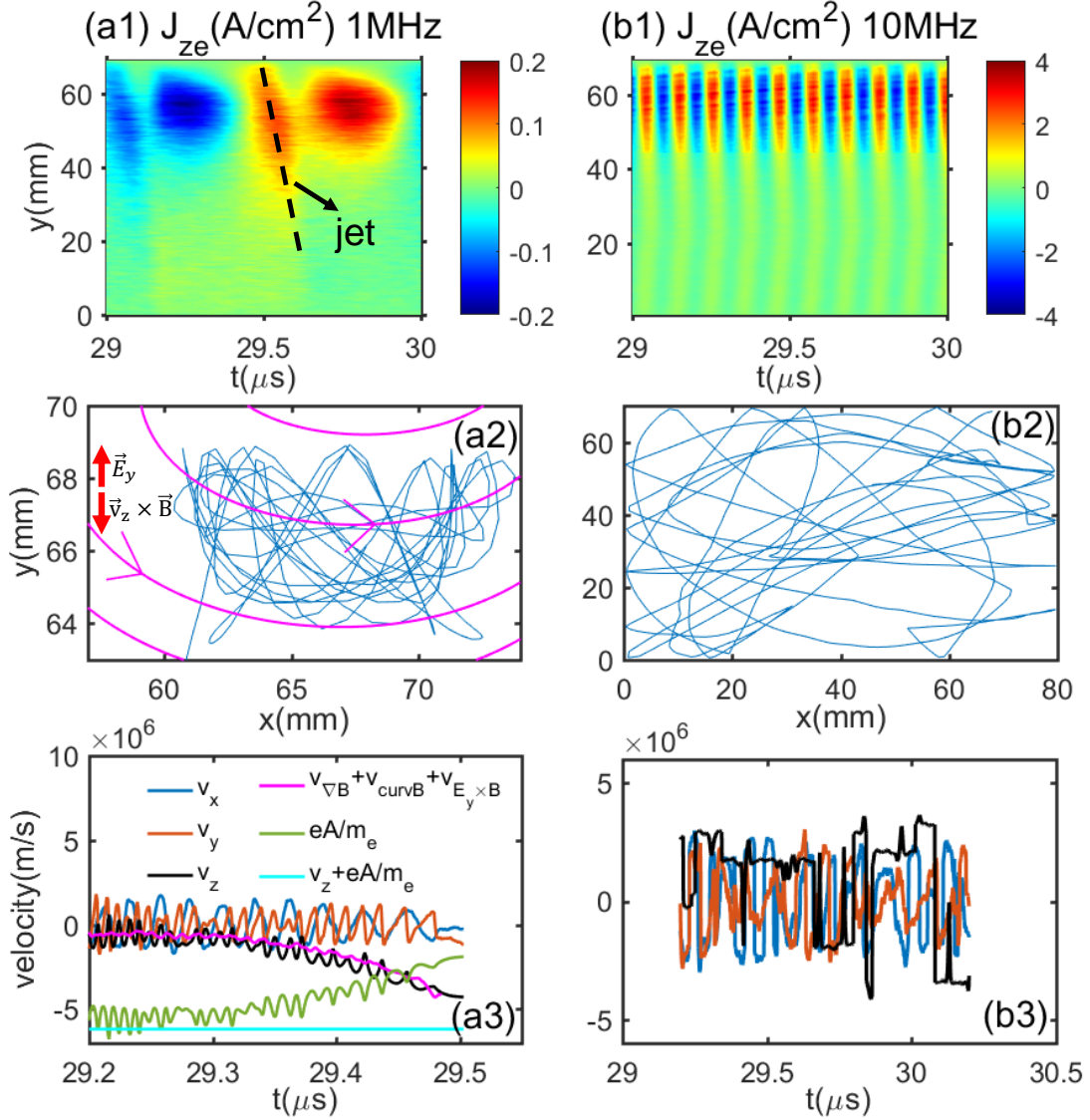


FIG. 2. Subplots (a1) and (b1) show the colormaps of the current density vs. y and t ; the cuts are taken along the black dashed lines in Fig. 1. Subplots (a2) and (b2) show representative particle trajectories, respectively, for the 1 MHz and 10 MHz cases over the time intervals denoted by subplots (a3) and (b3). The red arrows in (a2) denote the balance of electric force and Lorentz force for the test particle in 1 MHz case. Subplots (a3) and (b3) show the time dependence of the particle velocity and the drift velocity components, with $v_{\nabla B}$ being the drift due to magnetic field gradient, v_{curvB} being the curvature drift, and $v_{E_y \times B}$ being the $E_y \times B$ drift. The conservation of canonical momentum, eA and $m_e v_z + eA$ in 1 MHz case is illustrated by the green and light blue lines, respectively.

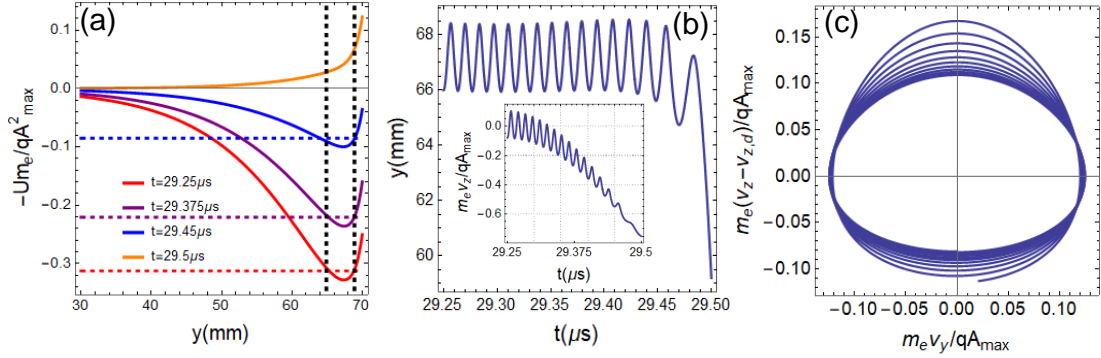


FIG. 3. Subplot (a) shows the time evolution of normalized effective potential U , where the horizontal dashed lines denote electron energy level and vertical dashed lines denote the electron turning points when being trapped in the effective potential well. Note at $t = 29.5\mu s$ the electron gets detrapped and leaves the skin layer towards bulk plasma. Subplots (b) and (c) show the phase space trajectories of an electron with initial velocity $v_{y0} = -0.1qA_{max}/m_e$, $v_{z0} = 0$, and initial position $y_0 = 66mm$. The velocity is normalized by $qA_{max}/m_e = 7 \times 10^6 m/s$.

y direction vanishes. In addition, the depth of the effective potential well where electrons are trapped also remains unchanged due to the Liouville theorem or conservation of the adiabatic moment, which is because of the slow variation of the effective potential compared to the bounce frequency. Correspondingly, the amplitude of v_y remains almost unchanged. When subtracting the drift velocity, $v_z - v_{z,d}$ changes over time, but not that different from a simple cyclotron motion in $v_y - v_z$ phase space (see Fig. 3 (c)), justifying the usage of cyclotron motion approximation used in the derivation of electron current below.

Although previous theory [61, 62] described certain aspects of this low frequency ICP regime, there are many new effects that were not described in these papers: notably the formation of jet like currents and a self-consistent value of the electric potential [61, 62] (see our accompanying paper Ref [78] for more details). Additionally, we observe that a large amount of electrons is produced by ionization near the coil and as we have shown, their motion can be treated as a cyclotron rotation around a guiding center combined with the drift in z direction. To obtain analytical solution to electron current, we describe the particle dynamics using a solution to the Vlasov equation by integrating it along the unperturbed particle trajectory. Two major assumptions are used: 1) The electron bounce frequency Ω is much higher than the driving frequency, ω , over most of the RF period. Indeed, for 1 MHz

case $\Omega_{max} \sim 10^8 \text{ s}^{-1}$ and $\omega = 6.28 \times 10^6 \text{ s}^{-1}$. 2) The plasma density and temperature profile gradients in the y direction are much larger than those in the x direction and we only solve a 1D system along the black dashed line in Fig. 1. Similar assumptions have been made by the pioneering paper of Tuszewski [9]. Under these assumptions, the kinetic equation for the perturbed electron distribution function is

$$\frac{\partial f_1}{\partial t} + \vec{v} \cdot \frac{\partial f_1}{\partial \vec{r}} + \frac{q}{m} (\vec{v} \times \vec{B} + \vec{E}_{sc}) \cdot \frac{\partial f_1}{\partial \vec{v}} = \frac{q}{m} \frac{\partial \vec{A}}{\partial t} \cdot \frac{\partial f_0}{\partial \vec{v}}, \quad (4)$$

where \vec{A} is the vector potential due to the coil current, f_0 is the background Maxwellian distribution, f_1 is the perturbation and E_{sc} is the in-plane electric field E_y coming from space charge separation. Essentially, we consider the case where RF magnetic field is dominant, which is the opposite limit of kinetic theories describing high frequency limits, see e.g., Ref. [38], where the RF magnetic field effects are neglected. Electron-neutral collisions are neglected since the collision frequency $\nu_{en} = 3.2 \times 10^6 \text{ s}^{-1} < \omega \ll \Omega_{max}$. Accounting for collisions is straightforward and we have verified that these weak collisions do not affect our results in a significant manner. The full derivation is given in our accompanying paper [78]. The total current in z direction contributed from f_0 and f_1 is

$$\vec{J}_{ze} = \int d\vec{v} (\vec{v}_{z,d} + \vec{v}_\perp) f_0 + \int d\vec{v} (\vec{v}_{z,d} + \vec{v}_\perp) f_1 = \vec{J}_{ze,0} + \vec{J}_{ze,1}, \quad (5)$$

where $\vec{v}_{z,d}$ is the drift in z direction and v_\perp is the perpendicular gyrovelocity. Upon integrating Eq. (4) along the unperturbed electron trajectory and making some justified assumptions, we obtain an analytical expression for \hat{f}_1 (f_1 in Fourier space). The current $J_{ze,1}$ is obtained from \hat{f}_1 as

$$J_{ze,1}(t) = Re \left\{ \sum_{k_y} \hat{J}_{ze,1}(t) e^{ik_y y} \right\} = Re \left\{ \sum_{k_y} \left[\frac{\omega q^2 N_e \hat{A}(t)}{T_e} v'_d \frac{v_F}{\omega} e^{-\xi} I_0(\xi) - \frac{i \omega q^2 N_e \hat{A}(t)}{T_e} \frac{(v'_d + v_F) k_y v_{th}^2}{\Omega \omega} e^{-\xi} (I_0(\xi) - I'_0(\xi)) - \frac{\omega q^2 N_e \hat{A}(t)}{T_e} \frac{v_{th}^2}{\omega} e^{-\xi} (2\xi I_0(\xi) - 2\xi I'_0(\xi)) \right] e^{ik_y y} \right\}, \quad (6)$$

where $Re \{ \dots \}$ denotes the real part, $\hat{J}_{ze,1}$ and \hat{A} denote the Fourier components, N_e is the electron density, T_e is the electron temperature, $\Omega(t) \approx qB(t)/m_e$, $v_F \approx -\langle F \rangle / qB(t) + E_y / B(t)$ is the total electron drift velocity, $\langle F \rangle = -\langle m_e (v_\perp^2 / 2 + v_\parallel^2) \rangle \nabla_\perp \ln B$ is the average force (over particles) due to the magnetic field gradient and curvature, v_\perp and v_\parallel are

the gyro-velocity perpendicular to and velocity parallel to the magnetic field, I_0 is the 0's order modified Bessel function of the first kind (the prime on it denotes derivative), $\xi = (k_y v_{th}/\Omega(t))^2$, where k_y denotes the wave vector of the vector potential A , and the diamagnetic drift velocity is $v'_d \approx T_e/qB(t)d\ln N_e/dy$. The first term in Eq. (6) is due to the electron drifts $\vec{v}_{z,d}$ whereas the second and third terms represent contribution from \vec{v}_\perp , which is response to the RF electromagnetic field modified by gyro-motion. The current contributed from f_0 is

$$J_{ze,0}(t) = qN_e v_F \left(1 - \exp\left(-\frac{1}{2} \frac{v_{\perp,tr}^2}{v_{th}^2}\right) \right), \quad (7)$$

where $v_{\perp,tr} = qB(t)\delta/2m_e$ is the maximum perpendicular velocity for the electrons to be trapped in the effective potential well (see Eq. (9)), since only the trapped electrons in f_0 contributes to current.

Our case is more complicated than the usual gyrokinetics [80, 81] in two aspects. First, only electrons are magnetized, so the current from electron $E \times B$ drift dominates and cannot be canceled with that of the ions. Second, the drift velocity v_F is comparable to or larger than the thermal velocity v_{th} , making the terms associated with v_F dominant. Neglecting the small second and third term in Eq. (6), and considering $e^{-\xi} I_0(\xi) \approx 1/\sqrt{2\pi\xi}$ (a good approximation as long as $\xi > 0.3$, which is almost always true for the cases that we are considering here), the amplitude of total current in Eq. (5) can be estimated to be

$$|J_{ze}| \approx |qN_e v_F + \frac{q^2 N_e E_z}{\omega T_e} \frac{v'_d v_F}{\sqrt{2\pi\xi}}| \sim \left| \frac{q^2 N_e E_z}{m_e \omega} - \frac{1}{\sqrt{2\pi}} \frac{q^3 N_e E_z^2}{v_{th} m_e^2 \omega^2} \right|, \quad (8)$$

where the factor $1/\sqrt{2\pi}$ comes from the finite Larmor radius effect, which reduces the current and $v_F \sim eA/m_e$ is used. At the black star in Fig. 1, the current amplitude estimated by Eq. (8) is $0.162A/cm^2$, approximately the same as the actual value $0.2A/cm^2$. Therefore, this expression can be used as an estimate of the amplitude of current in fluid codes and experiments. Physically, the dominance of RF magnetic field on particle motion changes the simple linear relation between electron current and RF electric field to be nonlinear, indicating the presence of a new physical regime. Since the maximum particle drift velocity $v_{F,max}$ for some electrons can be larger than the thermal velocity (see Fig. 2 (a3)), the contribution from f_1 to current is not negligible and $|J_{ze,1}| \sim 0.5|J_{ze,0}|$. With the gradual increase of coil current, the plasma density increases and the electron trajectory changes to the normal one seen in Fig. 2 (b3), making all drifts zero and the electron current becomes

the one predicted by previous kinetic theory $|J_{ze}| \sim |qN_e E_z|$. One can also prove that in this case, our new theory reduces to previous kinetic theory (see our accompanying paper).

Figure 4 compares the time evolution of J_{ze} and the energy deposition between theoretical predictions and PIC simulations. For our presently proposed theory (black) and the Tuszewski theory (red dashed) [9] that uses a simple fluid theory without taking into account self consistent electrostatic field, we evaluate the electric field and other relevant physical quantities at the location denoted by the black star in Fig. 1 (a4) and (b4). We then calculate the electron current from Eq. (5) and the conductivity given in Ref. [9], respectively. To carry out a calculation based on the previous non-local kinetic theory developed for high frequency ICP (blue), we employ the code provided in Ref. [38] to run a 2D simulation of the entire system, and then take electric field and electron current at the same location marked in Fig. 1 (a4), (b4). It is seen that fluid theory does predict the current and the energy deposition rate, whereas previous kinetic theory performs well only for the $f = 10$ MHz case. Our new theory, on the other hand, displays a much better agreement for both the current and the energy deposition at low frequency. We identify the new regime dominated by periodic bursty energy deposition as the “periodic burst regime”. The above comparison is performed at a single location because the electrons are trapped in the strong effective potential and the plasma response is nearly local. When averaging over the entire simulation domain, the jet-like current, comprised of the released trapped electrons (see Fig. 2 (a2)), contributes around 70% to the total energy deposition.

We perform a parameter scan over I_{coil} and ω to identify the boundary of the periodic burst regime. Figure 5 shows the average energy deposition, average ion density and average electron temperature for various coil parameters. We see that at lower frequencies there is a distinct jump in energy deposition from $10^{-2}W/cm^3$ to $10^0W/cm^3$, indicating a transition from the periodic burst regime to the anomalous (non-local) skin effect regime. A similar jump is observed for ion density and electron temperature. Physically, this transition occurs because in the periodic burst regime, the electric field and current are nearly out of phase during most of the RF period. This is because the strong RF magnetic field makes plasma response nearly local. Only in the phase of electron jet can one get significant energy deposition. Therefore, the effective energy deposition becomes much smaller than in the anomalous skin effect regime, making electron density also much smaller. Therefore, based on this understanding of particle dynamics, the criterion for transition between the

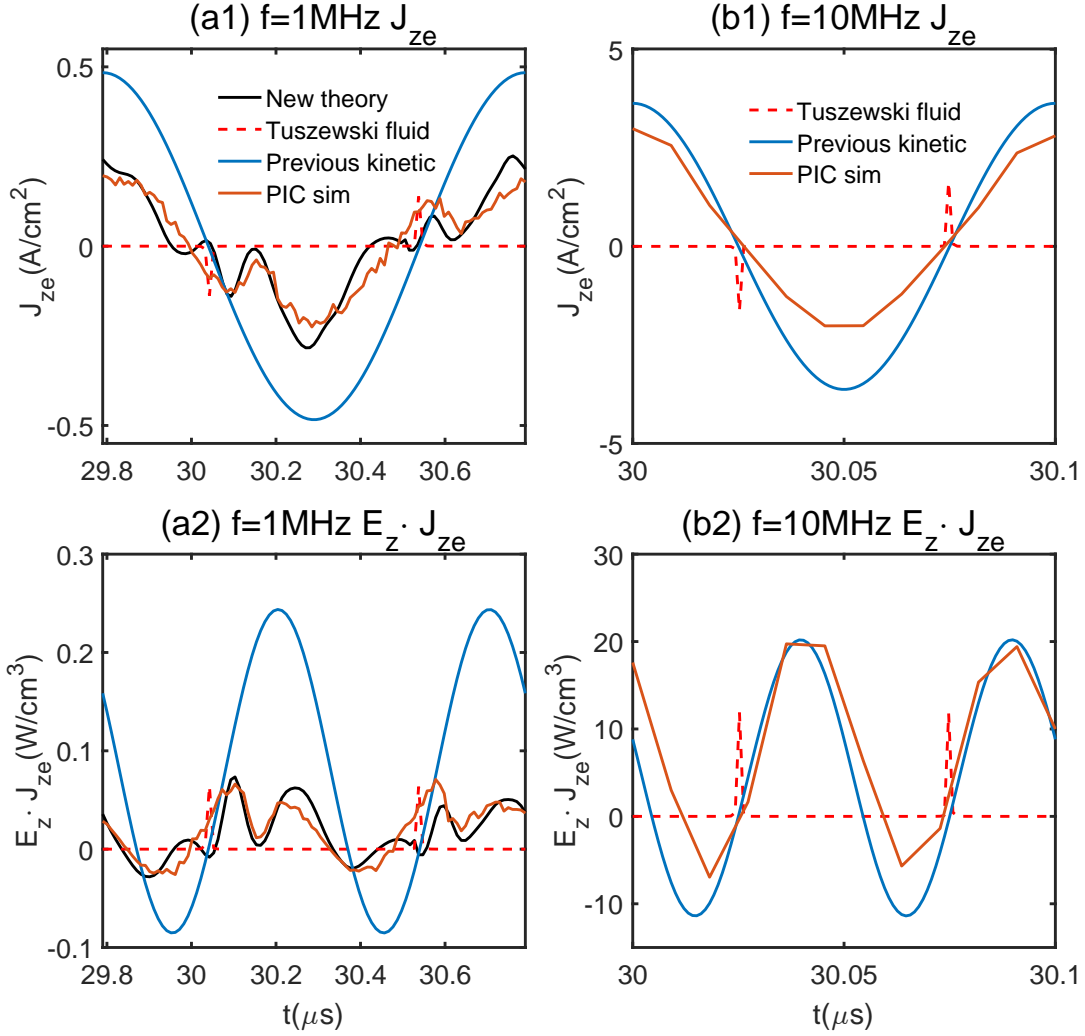


FIG. 4. Comparing PIC simulations with theory for panel (a) 1 MHz case and panel (b) 10 MHz case. Subplots (a1) and (b1) show the electron current J_{ze} , Subplots (a2) and (b2) show the energy deposition rate. The comparisons are made at spatial locations denoted by the black stars in Fig. 1 (a4) and (b4). We use Eq. (5) with $k_y = 2\pi n_y/L_y$ and $n_y = 1 \sim 210$ (region occupied by plasma). The fluid approach is from Ref. [9] and the non-local kinetic calculation is from Ref. [38].

bursty regime and the usual anomalous non-local regime can be estimated by equating twice the electron gyro-radius with the anomalous field skin depth (see more description in our accompanying paper):

$$2 \frac{m_e v_{th}}{qB} = \left(\frac{v_{th} c^2}{\omega \omega_{pe}^2} \right)^{1/3}. \quad (9)$$

When the diameter of the electron gyro-motion is larger than the skin depth, the electrons

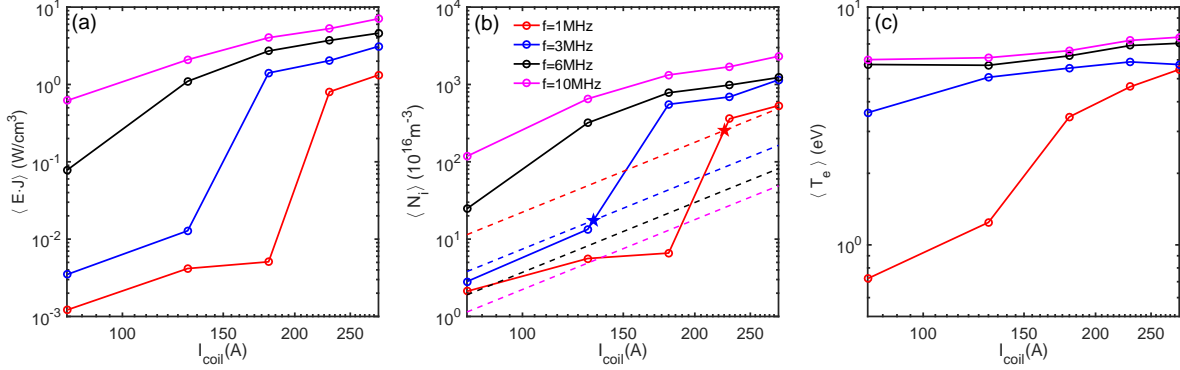


FIG. 5. The solid lines show, in a steady state, (a) energy deposition rates, averaged over entire simulation domain and one RF period, (b) time-averaged ion density at the probe location denoted by the black star in Fig. 1 (a3), and (c) time-averaged electron temperature at the same location, for different values of the coil current and driving frequency. The dashed lines denote the boundary for the onset of periodic burst regime, which follow a scaling law of $N_e \sim I_{coil}^3 / \omega T_e$ according to Eq. (9). Each dashed line denotes the boundary for same frequency as the solid line of the same color in the ion density plot. The red and blue stars in (b) denote the transition points of the two regimes.

are unlikely to undergo a full gyro-motion, and are therefore no longer being trapped in the RF effective potential. Based on Eq. (9), an estimate of the threshold plasma density defining the boundary of the periodic burst regime is obtained. The cases with different driving frequencies will have different transition values for the plasma density, as indicated in Fig. 5 (b) by the dashed lines. One expects to obtain the periodic burst regime in the region below the dashed lines. A reasonable agreement is found, with the red and blue stars in (b) denoting the transition point, indicating the validity of Eq. (9) in estimating the boundary between periodic burst regime and anomalous non-local regime.

Conclusions—We identify a periodic bursty energy deposition regime in low frequency ICP discharges where the electrons are magnetized and their dynamics are dominated by the bounce in the RF effective potential during most of the RF period, so that the electron response becomes nearly local in space. When the RF magnetic field becomes weak, the electrons demagnetize, forming a jet-like current which propagates quickly into the plasma and accounts for a significant fraction of the energy deposition. A new kinetic theory is proposed to estimate the electron current, which is in good agreement with particle-in-cell

simulations. A new nonlinear relation between the magnitude of the electron current and the amplitude of RF electric field is proposed. The condition in the ICP parameter space for the transition from normal (unmagnetized electrons) to the periodic burst regime is identified as a result of analysis of data produced in a series of 2D simulations and is also analytically derived. A significant density jump in the plasma density is observed during such transition, akin to what was observed in the E-H mode transition [12, 77, 82–84]. Therefore, our finding also offers a new possible explanation to the density jumps in the transition between E-mode and H-mode in low-frequency, low pressure ICP. We propose a simple estimate for amplitude of current density in plasma skin region (Eq. (8)) and a criterion for transition to the periodic burst regime (Eq. (9)) that can be verified in future experiments.

Acknowledgement– The authors thank Dr. Edward Startsev for checking the derivations in this paper. The authors thank Dr. Sarvesh Sharma for the discussions of high frequency harmonics. The work was partially supported by the National Natural Science Foundation of China (Grant No. 12305223) and the National Natural Science Foundation of Guangdong Province (Grant No.2023A1515010762). This research was also supported in part by the U.S. Department of Energy, Office of Fusion Energy Science under Contract No. DE-AC02-09CH11466.

-
- [1] M. A. Lieberman and A. J. Lichtenberg, MRS Bulletin **30**, 899 (1994).
- [2] P. Chabert and N. Braithwaite, *Physics of Radio-Frequency Plasmas* (Cambridge University Press, 2011).
- [3] Y. Liu, Q. Zhang, W. Jiang, L. Hou, X. Jiang, W. Lu, and Y. Wang, Phys. Rev. Lett. **107**, 055002 (2011).
- [4] K. Zhao, D.-Q. Wen, Y.-X. Liu, M. A. Lieberman, D. J. Economou, and Y.-N. Wang, Phys. Rev. Lett. **122**, 185002 (2019).
- [5] T. Mussenbrock, R. P. Brinkmann, M. A. Lieberman, A. J. Lichtenberg, and E. Kawamura, Phys. Rev. Lett. **101**, 085004 (2008).
- [6] H. Sun, S. Banerjee, S. Sharma, A. T. Powis, A. V. Khrabrov, D. Sydorenko, J. Chen, and I. D. Kaganovich, Physics of Plasmas **30**, 103509 (2023).
- [7] J.-Y. Sun, F. Gao, F.-J. Zhou, J. Schulze, and Y.-N. Wang, Phys. Rev. Lett. **133**, 235302 (2024).
- [8] D. Yang, J. P. Verboncoeur, and Y. Fu, Phys. Rev. Lett. **134**, 045301 (2025).
- [9] M. Tuszewski, Phys. Rev. Lett. **77**, 1286 (1996).
- [10] Y. O. Tyshetskiy, A. I. Smolyakov, and V. A. Godyak, Phys. Rev. Lett. **90**, 255002 (2003).
- [11] H.-C. Lee, Applied Physics Reviews **5**, 011108 (2018).
- [12] Y. W. Lee, H. L. Lee, and T. H. Chung, Journal of Applied Physics **109**, 113302 (2011).
- [13] T. Piskin, Y. Qian, P. Pribyl, W. Gekelman, and M. J. Kushner, Journal of Applied Physics **133**, 173302 (2023).
- [14] E. Kawamura, M. Lieberman, and A. Lichtenberg, Physics of plasmas **13** (2006).
- [15] S. Sharma, S. Patil, S. Sengupta, A. Sen, A. Khrabrov, and I. Kaganovich, Physics of Plasmas **29** (2022).
- [16] H. Sun, J. Chen, I. D. Kaganovich, A. Khrabrov, and D. Sydorenko, Phys. Rev. E **106**, 035203 (2022).
- [17] H. Sun, J. Chen, I. D. Kaganovich, A. Khrabrov, and D. Sydorenko, Phys. Rev. Lett. **129**, 125001 (2022).
- [18] L. Xu, H. Sun, D. Eremin, S. Ganta, I. Kaganovich, K. Bera, S. Rauf, and X. Wu, Plasma Sources Science and Technology **32**, 105012 (2023).

- [19] O. Polomarov, C. Theodosiou, I. Kaganovich, D. Economou, and B. Ramamurthi, IEEE Transactions on Plasma Science **34**, 767 (2006).
- [20] H.-C. Lee, Applied Physics Reviews **5**, 011108 (2018).
- [21] V. I. Kolobov and D. J. Economou, Plasma Sources Science and Technology **6**, R1 (1997).
- [22] V. A. Godyak, R. B. Piejak, B. M. Alexandrovich, and V. I. Kolobov, Phys. Rev. Lett. **80**, 3264 (1998).
- [23] V. A. Godyak, R. B. Piejak, B. M. Alexandrovich, and V. I. Kolobov, Physics of Plasmas **6**, 1804 (1999).
- [24] V. Godyak, B. Alexandrovich, R. Piejak, and A. Smolyakov, Plasma Sources Science and Technology **9**, 541 (2000).
- [25] V. A. Godyak, B. M. Alexandrovich, and V. I. Kolobov, Phys. Rev. E **64**, 026406 (2001).
- [26] V. Godyak, R. Piejak, B. Alexandrovich, and A. Smolyakov, Plasma Sources Science and Technology **10**, 459 (2001).
- [27] F. F. Chen, Physics of Plasmas **8**, 3008 (2001).
- [28] J. D. Evans and F. F. Chen, Phys. Rev. Lett. **86**, 5502 (2001).
- [29] A. Smolyakov, V. Godyak, and A. Duffy, Physics of Plasmas **7**, 4755 (2000).
- [30] Y. O. Tyshetskiy, A. I. Smolyakov, and V. A. Godyak, Plasma Sources Science and Technology **11**, 203 (2002).
- [31] I. D. Kaganovich and O. Polomarov, Phys. Rev. E **68**, 026411 (2003).
- [32] I. Kaganovich, E. Startsev, and G. Shvets, Physics of Plasmas **11**, 3328 (2004).
- [33] I. D. Kaganovich, O. V. Polomarov, and C. E. Theodosiou, Physics of Plasmas **11**, 2399 (2004).
- [34] A. I. Smolyakov, V. A. Godyak, and Y. O. Tyshetskiy, Physics of Plasmas **10**, 2108 (2003).
- [35] H.-C. Lee, S. Oh, and C.-W. Chung, Plasma Sources Science and Technology **21**, 035003 (2012).
- [36] B. Ramamurthi, D. J. Economou, and I. D. Kaganovich, Plasma Sources Science and Technology **12**, 170 (2003).
- [37] A. M. Froese, *Particle-in-cell simulations of nonlocal and nonlinear effects in inductively coupled plasmas*, Ph.D. thesis, University of Saskatchewan (2007).
- [38] W. Yang and Y.-N. Wang, Plasma Physics and Controlled Fusion **63**, 035031 (2021).
- [39] W. Yang, F. Gao, and Y.-N. Wang, Physics of Plasmas **29**, 063503 (2022).

- [40] W. YANG, F. GAO, and Y. WANG, *Plasma Science and Technology* **24**, 055401 (2022).
- [41] W. Yang, F. Gao, and Y.-N. Wang, *AIP Advances* **12**, 055222 (2022).
- [42] W. Jiang, H. yu Wang, S. xia Zhao, and Y. nian Wang, *Journal of Physics D: Applied Physics* **42**, 102005 (2009).
- [43] H.-C. Lee, D.-H. Kim, and C.-W. Chung, *Applied Physics Letters* **102**, 234104 (2013).
- [44] I. M. El-Fayoumi and I. R. Jones, *Plasma Sources Science and Technology* **7**, 162 (1998).
- [45] S. Xu, K. N. Ostrikov, Y. Li, E. L. Tsakadze, and I. R. Jones, *Physics of Plasmas* **8**, 2549 (2001).
- [46] V. I. Kolobov and V. A. Godyak, *Plasma Sources Science and Technology* **26**, 075013 (2017).
- [47] F. Gao, H. Li, W. Yang, J. Liu, Y.-R. Zhang, and Y.-N. Wang, *Physics of Plasmas* **25**, 013515 (2018).
- [48] M. V. Isupov and V. A. Pinaev, *Journal of Applied Mechanics and Technical Physics* **64**, 757 (2023).
- [49] G. I. Sukhinin, M. V. Isupov, A. V. Fedoseev, and I. B. Yudin, *Journal of Physics: Conference Series* **1243**, 012004 (2019).
- [50] S. Ashida, M. R. Shim, and M. A. Lieberman, *Journal of Vacuum Science and Technology A* **14**, 391 (1996).
- [51] G. Cunge, B. Crowley, D. Vender, and M. M. Turner, *Plasma Sources Science and Technology* **8**, 576 (1999).
- [52] B. Ramamurthi and D. J. Economou, *Plasma Sources Science and Technology* **11**, 324 (2002).
- [53] P. Subramonium and M. J. Kushner, *Journal of Vacuum Science and Technology A: Vacuum, Surfaces, and Films* **20**, 325 (2002).
- [54] P. Subramonium and M. J. Kushner, *Journal of Vacuum Science and Technology A: Vacuum, Surfaces, and Films* **20**, 313 (2002).
- [55] S. Banna, A. Agarwal, G. Cunge, M. Darnon, E. Pargon, and O. Joubert, *Journal of Vacuum Science and Technology A* **30** (2012).
- [56] Y. Qian, W. Gekelman, P. Pribyl, T. Piskin, and A. Paterson, *Physics of Plasmas* **31**, 063507 (2024).
- [57] U. Fantz, H. Falter, P. Franzen, D. Wunderlich, M. Berger, A. Lorenz, W. Kraus, P. McNeely, R. Riedl, and E. Speth, *Nuclear fusion* **46**, S297 (2006).
- [58] E. Speth, H. Falter, P. Franzen, U. Fantz, M. Bandyopadhyay, S. Christ, A. Encheva,

- M. Fröschle, D. Holtum, B. Heinemann, *et al.*, Nuclear Fusion **46**, S220 (2006).
- [59] H. Li, F. Gao, D.-Q. Wen, W. Yang, P.-C. Du, and Y.-N. Wang, Journal of Applied Physics **125**, 173303 (2019).
- [60] D. Zielke, S. Briefi, S. Lishev, and U. Fantz, Plasma Sources Science and Technology **31**, 035019 (2022).
- [61] R. H. Cohen and T. D. Rognlien, Physics of Plasmas **3**, 1839 (1996).
- [62] R. H. Cohen and T. D. Rognlien, Plasma Sources Science and Technology **5**, 442 (1996).
- [63] A. M. Froese, A. I. Smolyakov, and D. Sydorenko, Physics of Plasmas **16**, 080704 (2009).
- [64] M. R. Gibbons and D. W. Hewett, Journal of Computational Physics **120**, 231 (1995).
- [65] M. M. Turner, Plasma Sources Science and Technology **5**, 159 (1996).
- [66] D. Y. Sydorenko, A. I. Smolyakov, Y. O. Tyshetskiy, and V. A. Godyak, Physics of Plasmas **12**, 033503 (2005).
- [67] C. Fu, Y. Dong, Y. Li, W. Wang, Z. Wang, and W. Liu, Journal of Physics D: Applied Physics **57**, 135201 (2024).
- [68] H. Wen, J. Schulze, Y. Fu, J.-Y. Sun, and Q.-Z. Zhang, Plasma Sources Science and Technology **34**, 03LT01 (2025).
- [69] T. Charoy, J.-P. Boeuf, A. Bourdon, J. A. Carlsson, P. Chabert, B. Cuenot, D. Eremin, L. Garrigues, K. Hara, I. D. Kaganovich, *et al.*, Plasma Sources Science and Technology **28**, 105010 (2019).
- [70] B. Jin, J. Chen, A. V. Khrabrov, Z. Wang, and L. Xu, Plasma Sources Science and Technology **31**, 115015 (2022).
- [71] Q. Cao, J. Chen, H. Sun, G. Sun, S. Liu, C. Tan, and Z. Wang, Physics of Plasmas **30**, 103501 (2023).
- [72] J. Chen, A. V. Khrabrov, I. D. Kaganovich, and H.-P. Li, Physics of Plasmas **31**, 042112 (2024).
- [73] B. Jin, J. Chen, G. Sun, Z. Wang, and H. Sun, Plasma Sources Science and Technology **33**, 06LT01 (2024).
- [74] D. Sydorenko and I. Kaganovich, Physics of Plasmas (2024).
- [75] B. I. Cohen, A. Langdon, and A. Friedman, Journal of Computational Physics **46**, 15 (1982).
- [76] D. Sydorenko, I. D. Kaganovich, A. V. Khrabrov, S. A. Ethier, J. Chen, and S. Janhunen, Improved algorithm for a two-dimensional darwin particle-in-cell code (2024), arXiv:2409.19559

[physics.plasm-ph].

- [77] S. Mattei, K. Nishida, S. Mochizuki, A. Grudiev, J. Lettry, M. Q. Tran, and A. Hatayama, *Plasma Sources Science and Technology* **25**, 065001 (2016).
- [78] H. Sun, J. Chen, A. Khrabrov, I. D. Kaganovich, W. Yang, D. Sydorenko, and S. Brunner, To be submitted (2025).
- [79] See Supplemental Material at [URL will be inserted by publisher] for movie of nonlinear particle dynamics (2025).
- [80] W. W. Lee and H. Qin, *Physics of Plasmas* **10**, 3196 (2003).
- [81] J. R. Cary and A. J. Brizard, *Rev. Mod. Phys.* **81**, 693 (2009).
- [82] U. Kortshagen, N. D. Gibson, and J. E. Lawler, *Journal of Physics D: Applied Physics* **29**, 1224 (1996).
- [83] P. Chabert, A. J. Lichtenberg, M. A. Lieberman, and A. M. Marakhtanov, *Journal of Applied Physics* **94**, 831 (2003).
- [84] T. Wegner, C. Küllig, and J. Meichsner, *Plasma Sources Science and Technology* **26**, 025007 (2017).